Theory-restricted resonant x-ray reflectometry of quantum materials

Katrin Fürsich,[1,*] Volodymyr B. Zabolotnyy,[1,†] Enrico Schierle,[2] Lenart Dudy,[1] Ozan Kirilmaz,[1] Michael Sing,[1] Ralph Claessen,[1] Robert J. Green,[3,4] Maurits W. Haverkort,[5] and Vladimir Hinkov[1,‡]

[1]*Physikalisches Institut and Röntgen Center for Complex Material Systems, Universität Würzburg, 97074 Würzburg, Germany*

[2]*Helmholtz-Zentrum Berlin für Materialien und Energie GmbH (HZB), 12489 Berlin, Germany*

[3]*Stewart Blusson Quantum Matter Institute, University of British Columbia, Vancouver V6T 1Z4, Canada*

[4]*Department of Physics & Engineering Physics, University of Saskatchewan, Saskatoon, Saskatchewan S7N 5E2, Canada*

[5]*Institut für Theoretische Physik, Universität Heidelberg, 69120 Heidelberg, Germany*

(Received 12 December 2017; published 16 April 2018)

The delicate interplay of competing phases in quantum materials is dominated by parameters such as the crystal field potential, the spin-orbit coupling, and, in particular, the electronic correlation strength. Whereas small quantitative variations of the parameter values can thus qualitatively change the material, these values can hitherto hardly be obtained with reasonable precision, be it theoretically or experimentally. Here we propose a solution combining resonant x-ray reflectivity (RXR) with multiplet ligand field theory (MLFT). We first perform *ab initio* DFT calculations within the MLFT framework to get initial parameter values, which we then use in a fit of the theoretical model to RXR. To validate our method, we apply it to NiO and $SrTiO_3$ and obtain parameter values, which are amended by as much as 20% compared to the *ab initio* results. Our approach is particularly useful to investigate topologically trivial and nontrivial correlated insulators, staggered moments in magnetically or orbitally ordered materials, and reconstructed interfaces.

DOI: 10.1103/PhysRevB.97.165126

I. INTRODUCTION

Quantum materials can host a variety of magnetic, orbitally ordered, superconducting, and topologically trivial or nontrivial correlated insulating phases [1–3]. The properties of these phases, and the phase diagrams resulting from their competition, mainly depend on the electronic correlation strength, along with a few further microscopic parameters such as the spin-orbit (SO) interaction energies, crystal field (CF) potentials, and hopping integrals. For instance, knowledge of the correlation strength is crucial to explain why NiO is an insulator, or to assess the various theories of superconductivity in cuprates and pnictides [1,2]; the energy-scale ratio of correlations, SO interactions, and hopping controls the phase diagrams of topological insulators [3]; and, finally, the energy scales of the CF splitting and the correlation-based Hund's first rule are so closely balanced in $LaCoO_3$ that meV temperature variations and strain of $\sim$1.5% drive a transition from a spin 0 to a robust magnetic state [4].

Whereas tiny variations of the parameter values can thus fundamentally change the material properties, no universal method exists to quantify these values with reasonable precision. A promising idea is to combine resonant x-ray methods such as x-ray absorption spectroscopy (XAS) [5] with theory [6–8]. Endeavours so far broadly fall into two categories. In predominantly theoretical work, predictions are made about the parameter values and the resulting spectra are compared to experimental data. Examples include quantum chemistry [9,10] or configuration interaction studies [11], and our combination of multiplet-ligand-field theory (MLFT) [12] with *ab initio* density-functional theory.

Although assessing the theory, such comparisons do not directly improve it. The alternative approach of fitting the parameters to experimental data [13,14] entails different problems. Typically, only the parameters of interest are fitted, while the others are determined by often less specific methods, making it difficult to ascertain an overall physical result. In addition, the routinely used XAS is prone to quantitative distortions [5].

Here we present a hybrid approach, which largely eliminates these drawbacks. We use resonant x-ray reflectivity (RXR) data, providing more detailed, quantitative information. We model the spectra within a comprehensive MLFT-based theory [12] by first calculating all its relevant parameters *ab initio* and then using them as initial values for a fit to the spectra. We validate our approach by applying it to two prototypical transition-metal oxides, $SrTiO_3$ (STO) and NiO, which yields excellent fits with parameter values amended by up to 20% as compared to the theoretical predictions.

II. EXPERIMENTAL METHODS

Both XAS and RXR depend on the atomic scattering factors $f(E) = f_1(E) + if_2(E)$. Concentrated to the vicinity of the absorption edges, $f(E)$ contains all the information to extract the microscopic properties of each element within its crystalline surroundings.

*Present address: Max-Planck-Institute for Solid State Research, Heisenbergstraße 1, 70569 Stuttgart, Germany.

†volodymyr.zabolotnyy@physik.uni-wuerzburg.de

‡hinkov@physik.uni-wuerzburg.de

TABLE I. MLFT parameters for NiO and $SrTiO_3$. The starting values were obtained theoretically (Ref. [12]) and used for the theory-restricted fit to the RXR data. The values $U_{dd} = 7.3$, $U_{pd} = 8.5$, and $\Delta = 4.7$ (NiO), and $U_{dd} = 6.0$, $U_{pd} = 8.0$, and $\Delta = 6.0$ (STO) are fixed following Ref. [12]. All values are in eV.

	10Dq	T_{pp}	ζ_{3d}	$F^{(2)}_{dd}$	$F^{(4)}_{dd}$	ζ_{2p}	$F^{(2)}_{2p3d}$	$G^{(1)}_{2p3d}$	$G^{(3)}_{2p3d}$	V_{eg}	V_{t2g}
NiO, starting values	0.56	0.72	0.08	11.14	6.87	11.51	6.67	4.92	2.80	2.06	1.21
fitted values	0.50	0.74	0.10	12.51	7.72	11.32	7.49	5.53	3.15	1.88	1.26
STO, starting values	1.79	0.99	0.02	8.38	5.25	3.85	4.23	2.81	1.59	4.03	2.35
fitted values	1.47	0.81	0.02	8.72	5.46	3.79	4.40	2.92	1.65	3.59	2.72

The main advantages of XAS are the well-established experimental handling and the straightforward data analysis for bulk specimens [5]. To obtain $f_2(E) \propto \sigma_{\text{abs}}(E)$ in absolute units, where $\sigma_{\text{abs}}(E)$ is the absorption cross section, the resonant data is scaled to theoretical off-resonant values [15]. Then, the Kramers-Kronig relations are exploited to obtain $f_1(E)$.

XAS, however, also has several shortcomings. For instance, the electron and fluorescence yield techniques usually used to measure XAS [5,16–18] suffer from sample charging, self-absorption, and saturation. The latter can substantially change the ratio of the SO-split L_3 and L_2 peaks, invalidating dichroism measurements that rely on sum rules [18]. Saturation effects can be avoided by using inverse partial fluorescence yield [19]. Yet, uncertainties related to absolute unit normalization and the Kramers-Kronig transformation remain.

RXR, in contrast, which measures the reflected intensity $|R(q,E)|$, depends on the full, complex $f(E)$, is inherently self-normalizing, does not suffer from saturation or self absorption, and provides layer-resolved information (q is the z component of the scattering vector $\mathbf{q}$). For instance, for systems with known $f(E)$, it has been used to obtain element-specific concentration and valence state profiles [20–22], or to uncover electronic [21,23], orbital [24,25], and magnetic [26,27] reconstructions. In general, however, due to multiple scattering, due to the loss of phase information, and due to incomplete data sets and noise, the problem to invert $|R(q,E)|$ to obtain the complex refractive index $n(E,z) - 1 \propto f(E)c(z)$, and, subsequently, $f(E)$ is, in principle, ill-posed.

For reasonably well-known and simple chemical and electronic profiles $c(z)$, one can try to regularize the inversion problem by parameterizing $f(E)$ appropriately [28,29] and fitting it to the reflectivity data [30–32]. In Ref. [33], $f(E)$ was parameterized by a set of hundreds of triangular functions at the Ti L-edge in $SrTiO_3$. Whereas this approach allows one to address arbitrary $f(E)$, the problem remains strongly underconstrained due to the large number of parameters. Choosing appropriate starting values and constraining the deviation of the final results from these values by the maximum entropy method helps obtain reasonable results [33]. However, the choice of appropriate starting values requires substantial *a priori* knowledge of the very results to be found.

We introduce a different regularization method, which avoids these problems by parameterizing $f(E)$ using the relatively small set of parameters of MLFT [12]. Starting values are provided *ab initio* by the theory. Our approach has the additional advantage of directly yielding the values of the relevant microscopic parameters without a laborious interpretation of $f(E)$ in a separate step.

The investigated NiO film was grown using molecular-beam epitaxy. Ni metal was evaporated onto an epi-polished MgO substrate held at 200° C. An O_2 partial pressure of 7×10^{-7} mbar warranted fully oxidized NiO with no signatures of metallic Ni [34] in XAS. The growth rate was 1.5 Å NiO/min. Upon reaching ≈50 Å, the sample was transferred *in situ* into the RXR chamber. The investigated $SrTiO_3$ bulk sample with TiO_2 termination was prepared as described previously [35]. RXR and XAS data were collected at 300 K with σ-polarized light at the beamlines UE56-2 PGM-1 and UE46 PGM-1 at the Helmholtz-Zentrum Berlin.

III. MULTIPLET LIGAND FIELD THEORY

We use the program package Quanty [12,36] within the MLFT framework to evaluate the scattering factors

$$f_2(E) = \frac{\pi m E^2}{\hbar^2} \sum_f |\langle \Phi_i | \vec{\epsilon} \cdot \vec{r} | \Phi_f \rangle|^2 \, \delta(E_f - E_i - E),$$

where $\vec{\epsilon}$ is the light polarization and $|\Phi_i\rangle$ and $|\Phi_f\rangle$ are the initial and final many-particle states of the cluster, respectively, with energies E_i and E_f. We write $|\Phi_i\rangle$ and $|\Phi_f\rangle$ as multi-Slater determinants, represented in an orbital basis of Wannier functions, which can be expanded on radial wave functions times spherical harmonics centered at each atom in the cluster. In a basis including both the O-$2p$ and Ni-$3d$ Wannier orbitals, the latter are already quite well represented by a single $3d$ state multiplied with an atomiclike radial wave function. The O-$2p$ states need several expansion coefficients to be well represented. For an accurate description of the covalency and on-site energy it is, however, in all cases important to include the tails of the Wannier functions. For the core-to-valence transitions at the Ni site, it is sufficient to only include the core $2p$ and valence $3d$ angular momentum and the corresponding radial function. This reduces the number of three-dimensional integrals to be calculated to a single one-dimensional integral and we can write

$$\begin{aligned} f_2(E) = \frac{\pi m E^2}{\hbar^2} & |\langle R_{2p}(r)|r|R_{3d}(r)\rangle|^2 \\ & \times \sum_f |\langle \Psi_i(\theta,\varphi)|\vec{\epsilon} \cdot \hat{r}|\Psi_f(\theta,\varphi)\rangle|^2 \\ & \times \delta(E_f - E_i - E). \end{aligned}$$

MLFT depends on several microscopic parameters, such as multipole Coulomb and exchange interactions (Slater integrals) F and G determining the correlation strength, CF

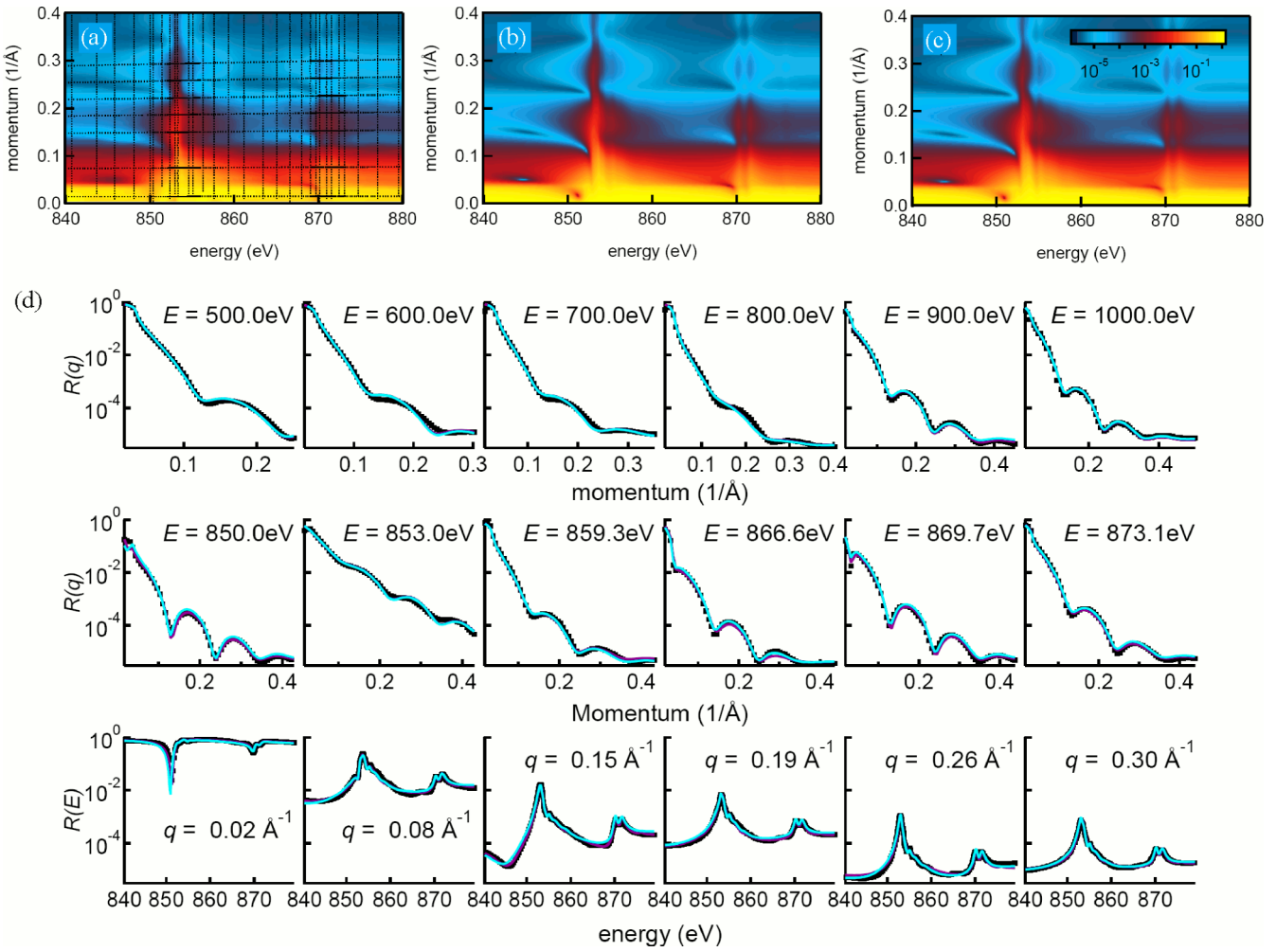

FIG. 1. Resonant x-ray reflectivity from the NiO sample. (a) Interpolated experimental map. Black dots mark data points. (b) Simulated reflectivity for the theory-based $f(E)$, using the final parameter values obtained by the fit described in the text. (c) Simulated reflectivity for the fitted Lorentzian-based $f(E)$. (d) Comparison between experimental (black squares) and fitted reflectivity [magenta: theory-based $f(E)$; cyan: Lorentzian-based $f(E)$].

potentials determining the on-site energies of the Ni-d and O-p orbitals ($10Dq$) as well as the hopping between them (T_{pp}, V_{eg}, V_{t2g}), and the SO-interaction energies (ζ_{3d}, ζ_{2p}). Their starting values for the subsequent fit are provided by *ab initio* cluster calculations [12] in the basis of the localized Wannier orbitals describing the DFT band structure (see Table I). Since the spherical part of the Coulomb repulsion U_{dd} and U_{pd}, and the charge transfer parameter Δ are not yet theoretically accessible with good precision, they were obtained from experimental data in Ref. [12]. In the absence of strong charge-transfer satellites sensitive to these parameters, we do not further refine their values here.

We keep the MLFT Hamiltonian tractable by not accounting for excitations into the continuum and for relaxation mechanisms of the excited states. Consequently, our final expression for $f_2(E)$ describes only the resonant contribution to the total $f(E)$ by providing the transition energies and their probabilities, assuming an infinite lifetime of the excited states. To compensate for that, we add the off-resonant part provided in Chantler tables [15] and introduce Lorentzian broadening [37]. Due to uncertainties in the edge positions [15], we allow small energy shifts and smooth the edges when matching the experimental data.

IV. RESULTS

We represent the depth-dependent chemical profile $c_i(z)$ of each element i by a set of layers, each with fitting parameters for roughness, thickness, and layer concentration, whose starting values are obtained from preliminary fits at off-resonant energies [20]. For most elements in our relatively simple samples, only one layer is necessary, and the concentration can be kept stoichiometric. The total number of these structural parameters is small and allows us to focus on the physical parameters.

In our analysis, we first concentrate on NiO. Using a combination of the Parratt formalism and differential evolution [20,38], we first fitted all the parameters (see Table I for the obtained values) to the experimental reflectivity $|R(q,E)|$. In Fig. 1, we compare $|R(q,E)|$ to simulations for the final set of fitted parameter values.

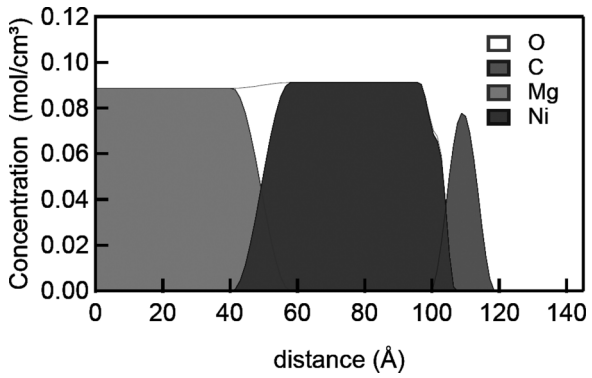

FIG. 2. Chemical profile showing the depth distribution of the elements in the NiO sample resulting from the fits.

The resulting chemical profile is shown in Fig. 2, demonstrating that we indeed have a single NiO film with smooth interfaces. A thin layer accounts for residual organic surface contaminations [20]. Finally, the fitted scattering factor in the vicinity of the Ni resonance is shown in Fig. 3(a).

A major motivation to restrict the fit based on theoretical considerations was to avoid underdetermination. To demonstrate that the solution has not become overconstrained instead, we have performed a second fit, in which $f(E)$ was modeled by a set of N Lorentzians $A_n/(E - E_n + i\Gamma_n/2)$. To reproduce all details of background and resonant peaks, $N = 28$, such Lorentzians, with a large spread of widths, were used. The starting values for the parameters A_n, E_n, and Γ_n were obtained from XAS, and no restrictions were imposed. The free Lorentzian-based $f(E)$ resulting from this fit is essentially

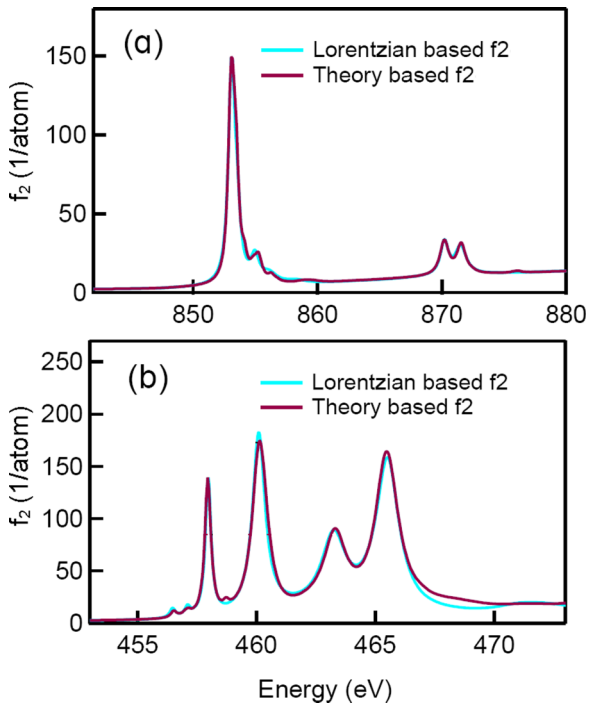

FIG. 3. Scattering factors based on fits to RXR. (a) NiO: $f_2(E)$ in the vicinity of the Ni L_3 and L_2 edges. (b) $SrTiO_3$: $f_2(E)$ in the vicinity of the Ti L_3 and L_2 edges.

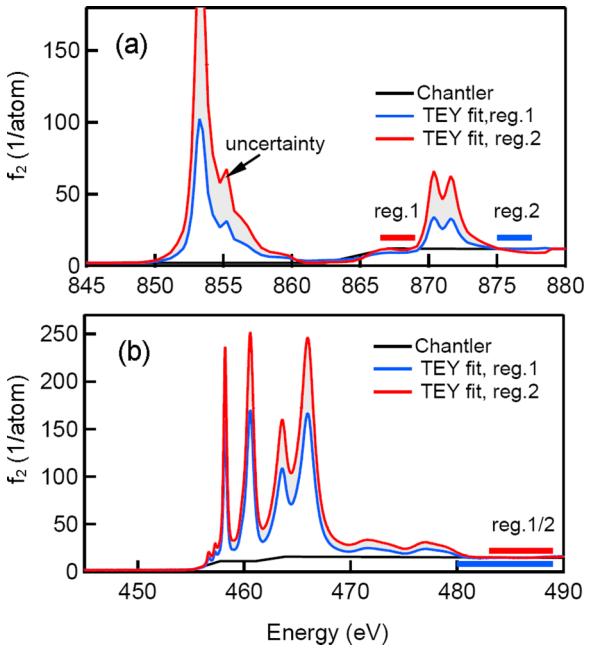

FIG. 4. Scattering factors derived from XAS in total electron yield mode. (a) NiO: $f_2(E)$ in the vicinity of the Ni L_3 and L_2 edges. Depending on the region, in which the data is scaled to fit the tabulated Chantler values [15], the result can vary between the two shown limiting cases. (b) $SrTiO_3$: $f_2(E)$ in the vicinity of the Ti L_3 and L_2 edges.

identical to the theory-restricted $f(E)$ [Fig. 3(a)], as are the corresponding simulated reflectivities [Figs. 1(b), 1(c) and 1(d)].

Despite the simple sample profile, determining $f(E)$ based on XAS alone is much more problematic: First, an uncertainty of up to a factor of two in the resonant amplitude results from the absolute unit scaling [Fig. 4(a)]. This is owed to noise and contributions from other physical processes in the off-resonant region [5], where data and tabulated values [15] are to be matched. Second, there is a substantial saturation-induced deviation of the L_3-L_2 ratio from the correct one obtained with RXR.

The entire approach was next applied to the STO sample. We show the resulting theory-restricted $f(E)$ around the Ti edge along with the nearly indistinguishable free Lorentzian-based $f(E)$ in Fig. 3(b). From Fig. 4(b), it is clear that an XAS-based approach is plagued by the same difficulties as for the NiO sample.

V. DISCUSSION AND OUTLOOK

For both materials, the fitted parameter values deviate by up to 20% from the theoretical starting values (see Table I). A quantitative correction of this magnitude will often qualitatively change the material properties, e.g., by tipping the balance towards a different phase than anticipated. In addition, these corrections allow us to identify and fix the shortcomings of our theory. In particular, our fit significantly improves the values of the Slater integrals $F^{(4)}_{dd}$, $F^{(2)}_{2p3d}$, $G^{(1)}_{2p3d}$, and $G^{(3)}_{2p3d}$, which describe the correlation strength. The theoretical

predictions underestimate their values since they do not take into account the core hole, whereas RXR probes a state in the presence of the core hole, which leads to wave-function contraction. For the same reason, theory predicts larger values for $10Dq$ and V_{eg} than experimentally obtained. In future investigations of materials with strong charge transfer satellites, Δ and U can be readily extracted from the fit as well [39].

Our approach brings unprecedented precision to the spectroscopic characterization already in bulk specimen. Yet, it will prove even more powerful for heterostructures: Interfaces frequently reconstruct, leading to strong depth modulations of the physical properties. The necessary layer-resolved analysis is already implemented in our method and was in fact exploited when modeling the different layers of the epitaxial NiO sample.

Already for the compositionally simple samples studied here, it was important to ensure that the problem does not become underconstrained. For heterostructures, which inherently have many more fitting parameters, a theory-restricted fitting procedure will be crucial to eliminate physically meaningless results.

Our approach can be readily applied to magnetic and orbitally ordered materials, by working with a tensorial rather than a scalar $f(E)$ to describe the dichroic material effects. The calculations [40] and RXR measurements [25,27] related to the corresponding matrix elements of $f(E)$ are of similar accuracy as in the isotropic case. This will be particularly useful when investigating the staggered magnetic moments of ferri- and antiferromagnets (a sufficiently short wavelength provided), where the site-averaging XAS cannot be exploited.

An experimentally optimized description of the local electronic structure within an MLFT framework has further benefits. As discussed, one can readily obtain several local expectation values such as ordered spin and orbital moments. These moments must be well defined as they are in principle given by sum rules over the atomic scattering factors; the advantage here is that one does not need to integrate, is not sensitive to offsets in background, and not hindered by theoretical approximations in deriving the sum rules [41]. Likewise, one has direct access to quantities such as covalence, charge fluctuations, orbital polarization, and ordering in a well-defined fashion.

ACKNOWLEDGMENTS

We are indebted to C. Schüßler-Langeheine for the preparation of the NiO samples, the provision of the reflectometry chamber used at UE56-2, as well as for support and discussions. We thank S. Macke for discussions. This paper has been financially supported by the German Research Foundation DFG through the Collaborative Research Center SFB 1170 "ToCoTronics" (Projects No. C04 and No. C08), the Natural Sciences and Engineering Research Council of Canada, and the Max-Planck-UBC Centre for Quantum Materials. We thank HZB for the allocation of synchrotron radiation beamtime and thankfully acknowledge the financial support by HZB.

[1] H. Y. Hwang, Y. Iwasa, M. Kawasaki, B. Keimer, N. Nagaosa, and Y. Tokura, Nat. Mater. **11**, 103 (2012).
[2] D. I. Khomskii, *Transition Metal Compounds* (Cambridge University Press, Cambridge, 2014).
[3] M. Hohenadler and F. F. Assaad, J. Phys.: Condens. Matter **25**, 143201 (2013).
[4] D. Fuchs, C. Pinta, T. Schwarz, P. Schweiss, P. Nagel, S. Schuppler, R. Schneider, M. Merz, G. Roth, and H. v. Löhneysen, Phys. Rev. B **75**, 144402 (2007).
[5] J. Stöhr, *NEXAFS Spectroscopy* (Springer, Berlin, Heidelberg, 2003).
[6] L. C. Davis, Phys. Rev. B **25**, 2912 (1982).
[7] G. van der Laan, J. Zaanen, G. A. Sawatzky, R. Karnatak, and J.-M. Esteva, Phys. Rev. B **33**, 4253 (1986).
[8] D. D. Sarma, N. Shanthi, S. R. Barman, N. Hamada, H. Sawada, and K. Terakura, Phys. Rev. Lett. **75**, 1126 (1995).
[9] L. Hozoi, L. Siurakshina, and J. van den Brink, Sci. Rep. **1**, 65 (2011).
[10] I. Josefsson, K. Kunnus, S. Schreck, A. Fölisch, F. de Groot, P. Wernet, and M. Odelius, J. Phys. Chem. Lett. **3**, 3565 (2012).
[11] H. Ikeno, I. Tanaka, Y. Koyama, T. Mizoguchi, and K. Ogasawara, Phys. Rev. B **72**, 075123 (2005).
[12] M. W. Haverkort, M. Zwierzycki, and O. K. Andersen, Phys. Rev. B **85**, 165113 (2012).
[13] D. Alders, L. H. Tjeng, F. C. Voogt, T. Hibma, G. A. Sawatzky, C. T. Chen, J. Vogel, M. Sacchi, and S. Iacobucci, Phys. Rev. B **57**, 11623 (1998).
[14] S. I. Csiszar, M. W. Haverkort, Z. Hu, A. Tanaka, H. H. Hsieh, H.-J. Lin, C. T. Chen, T. Hibma, and L. H. Tjeng, Phys. Rev. Lett. **95**, 187205 (2005).
[15] C. T. Chantler, J. Phys. Chem. Ref. Data **24**, 71 (1995).
[16] M. Pompa, A. M. Flank, P. Lagarde, J. C. Rife, I. Stekhin, M. Nakazawa, H. Ogasawara, and A. Kotani, Phys. Rev. B **56**, 2267 (1997).
[17] F. de Groot, M. Arrio, P. Sainctavit, C. Cartier, and C. Chen, Solid State Commun. **92**, 991 (1994).
[18] R. Nakajima, J. Stöhr, and Y. U. Idzerda, Phys. Rev. B **59**, 6421 (1999).
[19] A. J. Achkar, T. Z. Regier, H. Wadati, Y.-J. Kim, H. Zhang, and D. G. Hawthorn, Phys. Rev. B **83**, 081106(R) (2011).
[20] S. Macke, A. Radi, J. E. Hamann-Borrero, V. A., M. Bluschke, S. Brück, E. Goering, R. Sutarto, F. He, G. Cristiani, M. Wu, E. Benckiser, H.-U. Habermeier, G. Logvenov, N. Gauquelin, G. A. Botton, A. P. Kajdos, S. Stemmer, G. A. Sawatzky, M. W. Haverkort, B. Keimer, and V. Hinkov, Adv. Mater. **26**, 6554 (2014).
[21] J. E. Hamann-Borrero, S. Macke, W. S. Choi, R. Sutarto, F. He, A. Radi, I. Elfimov, R. J. Green, M. W. Haverkort, V. B. Zabolotnyy, H. N. Lee, G. A. Sawatzky, and V. Hinkov, NPJ Quantum Mater. **1**, 16013 (2016).
[22] V. B. Zabolotnyy, K. Fürsich, R. J. Green, P. Lutz, K. Treiber, C.-H. Min, A. V. Dukhnenko, N. Y. Shitsevalova, V. B. Filipov, B. Y. Kang, B. K. Cho, R. Sutarto, F. He, F. Reinert, D. S. Inosov, and V. Hinkov, arXiv:1801.03315.
[23] S. Smadici, P. Abbamonte, A. Bhattacharya, X. Zhai, B. Jiang, A. Rusydi, J. N. Eckstein, S. D. Bader, and J. M. Zuo, Phys. Rev. Lett. **99**, 196404 (2007).
[24] M. Salluzzo, J. C. Cezar, N. B. Brookes, V. Bisogni, G. M. De Luca, C. Richter, S. Thiel, J. Mannhart, M. Huijben, A.

Brinkman, G. Rijnders, and G. Ghiringhelli, Phys. Rev. Lett. **102**, 166804 (2009).

[25] E. Benckiser, M. W. Haverkort, S. Brück, E. Goering, S. Macke, A. Frañó, X. Yang, O. K. Andersen, G. Cristiani, H.-U. Habermeier, A. V. Boris, I. Zegkinoglou, P. Wochner, H.-J. Kim, V. Hinkov, and B. Keimer, Nat. Mater. **10**, 189 (2011).

[26] J. M. Tonnerre, M. De Santis, S. Grenier, H. C. N. Tolentino, V. Langlais, E. Bontempi, M. Garcia-Fernandez, and U. Staub, Phys. Rev. Lett. **100**, 157202 (2008).

[27] S. Macke and E. Goering, J. Phys.: Condens. Matter **26**, 363201 (2014).

[28] A. B. Kuzmenko, Rev. Sci. Instrum. **76**, 083108 (2005).

[29] S. M. Valvidares, M. Huijben, P. Yu, R. Ramesh, and J. B. Kortright, Phys. Rev. B **82**, 235410 (2010).

[30] J. Schlappa, C. F. Chang, Z. Hu, E. Schierle, H. Ott, E. Weschke, G. Kaindl, M. Huijben, G. Rijnders, D. H. A. Blank, L. H. Tjeng, and Schüßler-Langeheine, J. Phys.: Condens. Matter **24**, 035501 (2012).

[31] R. Storn and K. Price, J. Global Optim. **11**, 341 (1997).

[32] M. Björck and G. Andersson, J. Appl. Crystallogr. **40**, 1174 (2007).

[33] K. H. Stone, S. M. Valvidares, and J. B. Kortright, Phys. Rev. B **86**, 024102 (2012).

[34] T. J. Regan, H. Ohldag, C. Stamm, F. Nolting, J. Lüning, J. Stöhr, and R. L. White, Phys. Rev. B **64**, 214422 (2001).

[35] L. Dudy, M. Sing, P. Scheiderer, J. D. Denlinger, P. Schütz, J. Gabel, M. Buchwald, C. Schlueter, T.-L. Lee, and R. Claessen, Adv. Mater. **28**, 7443 (2016).

[36] M. W. Haverkort, Quanty—a quantum many body script language (2016), http://www.quanty.org.

[37] E. Stavitski and F. M. F. de Groot, Micron **41**, 687 (2010).

[38] L. G. Parratt, Phys. Rev. **95**, 359 (1954).

[39] E. C. Wasinger, F. M. F. de Groot, B. Hermann, K. O. Hodgson, and E. I. Solomon, J. Am. Chem. Soc. **125**, 12894 (2003).

[40] M. W. Haverkort, N. Hollmann, I. P. Krug, and A. Tanaka, Phys. Rev. B **82**, 094403 (2010).

[41] C. T. Chen, Y. U. Idzerda, H.-J. Lin, N. V. Smith, G. Meigs, E. Chaban, G. H. Ho, E. Pellegrin, and F. Sette, Phys. Rev. Lett. **75**, 152 (1995).